Supplementary Information for "Paleoclimate pattern effects strongly constrain modern climate sensitivity and 21st-century warming"

V. T. Cooper[1], K. C. Armour[1,2], G. J. Hakim[1], J. E. Tierney[3], N. J. Burls[4], C. Proistosescu[5], T. Andrews[6,7], W. Dong[8,9], M. T. Dvorak[2], R. Feng[10], M. B. Osman[11], Y. Dong[12]

[1]Department of Atmospheric and Climate Science, University of Washington, Seattle, WA, USA

[2]School of Oceanography, University of Washington, Seattle, WA, USA

[3]Department of Geosciences, University of Arizona, Tucson, AZ, USA

[4]Department of Atmospheric, Oceanic and Earth Sciences, George Mason University, Fairfax, VA, USA

[5]Department of Climate, Meteorology, and Atmospheric Sciences, University of Illinois at Urbana-Champaign, Champaign, IL, USA

[6]Met Office Hadley Centre, Exeter, UK

[7]School of Earth and Environment, University of Leeds, Leeds, UK

[8]Cooperative Programs for the Advancement of Earth System Science, University Corporation for Atmospheric Research, Boulder, CO, USA

[9]NOAA/Geophysical Fluid Dynamics Laboratory, Princeton, NJ, USA

[10]Department of Geosciences, University of Connecticut, Storrs, CT, USA

[11]Department of Geography, The University of Cambridge, Cambridge, UK

[12]Department of Atmospheric and Oceanic Sciences, University of California Los Angeles, Los Angeles, CA, USA

Contents of this file

Corresponding author: Vincent T. Cooper, Department of Atmospheric and Climate Science, University of Washington, Seattle, Washington, USA. (vcooper@uw.edu)

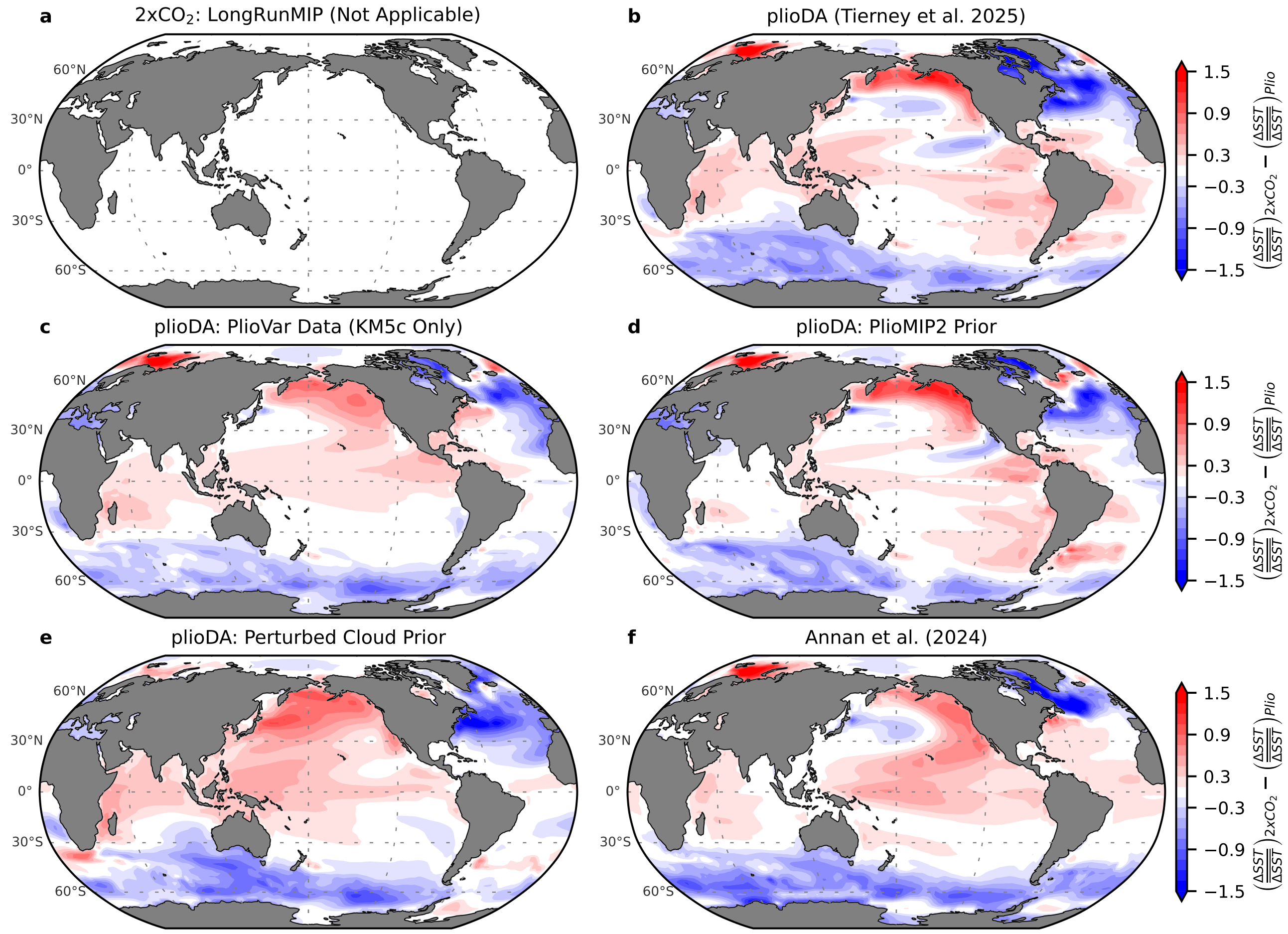

Figure S1. Differences between the 2xCO_2 pattern of sea-surface temperature (SST) anomalies and Pliocene patterns of SST anomalies. Panels correspond to Figure 1 of Main Text. Before taking the differences, each pattern's local anomalies are divided by its global-mean SST anomaly to emphasize the spatial patterns. Red regions indicate stronger relative amplification of warming in the LongRunMIP 2xCO_2 pattern (Rugenstein et al., 2019), while blue regions indicate stronger relative amplification of Pliocene warming. See Figure S10 for zonal-mean SST anomalies and pattern differences.

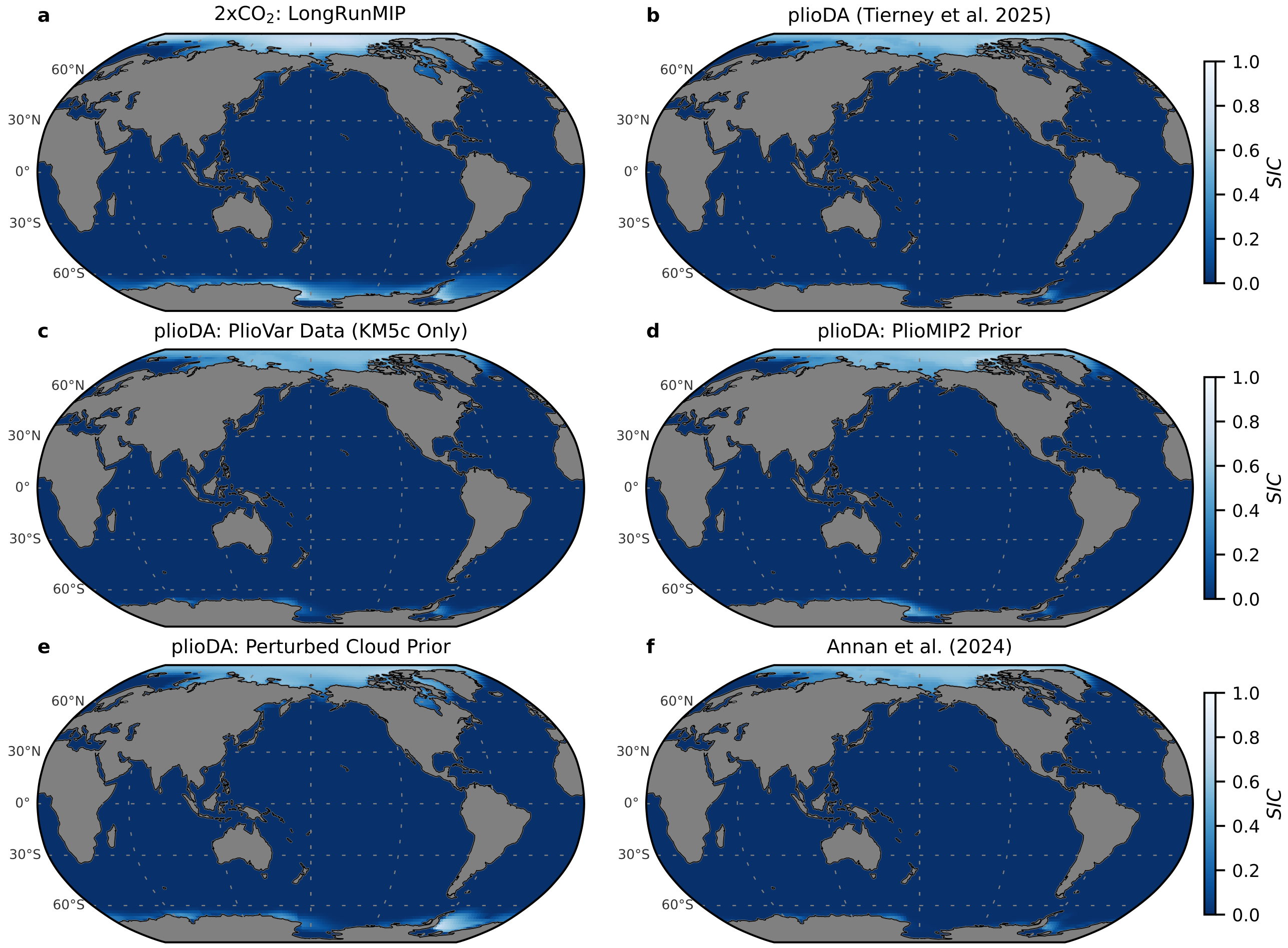

Figure S2. Sea-ice concentration (SIC): LongRunMIP 2xCO_2 and Pliocene reconstructions. Panels show annual-mean. Note that plioDA sea ice is used for the Annan et al. (2024) reconstruction.

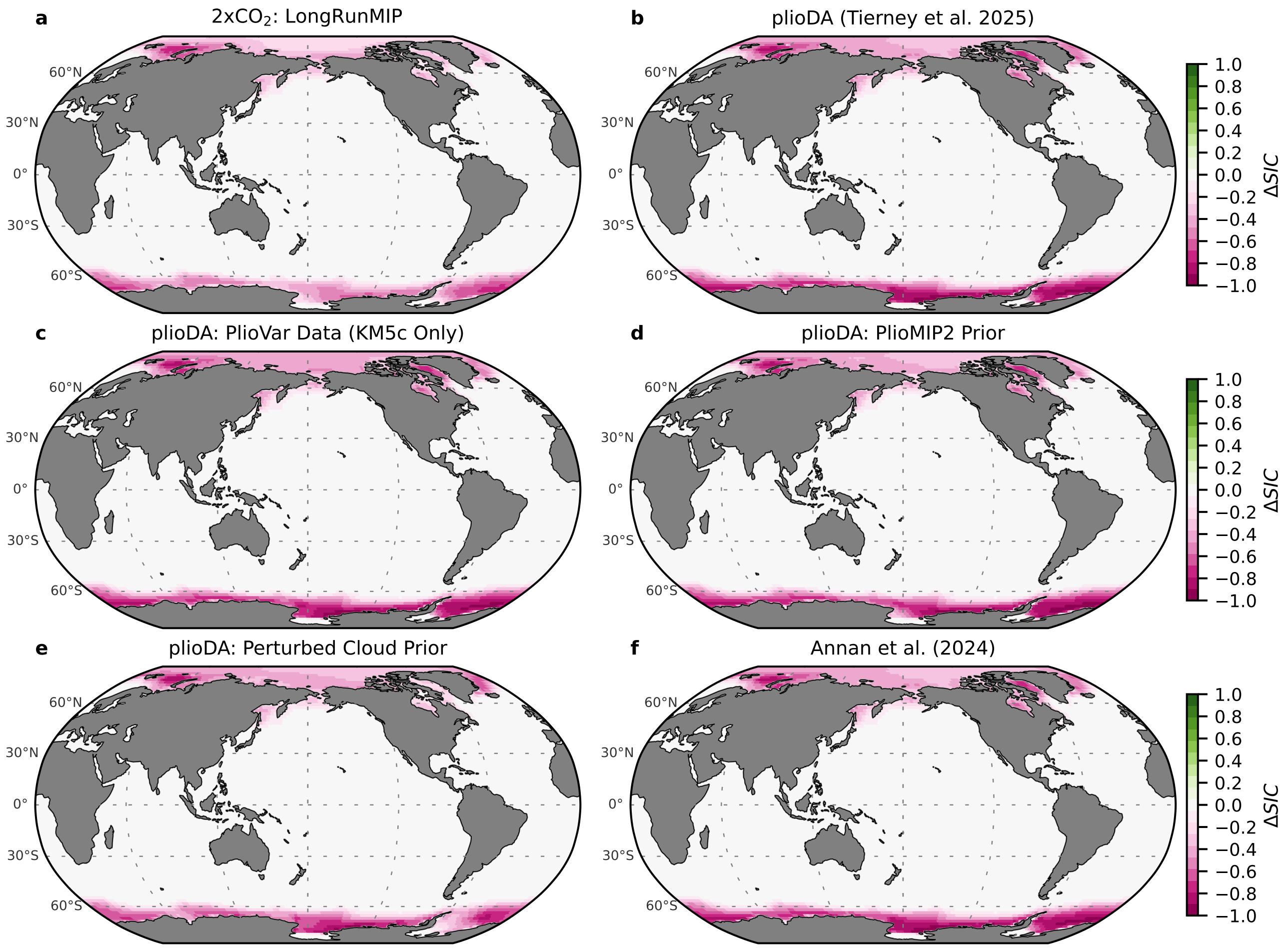

Figure S3. Sea-ice concentration (SIC) anomalies: LongRunMIP 2xCO_2 and Pliocene reconstructions relative to preindustrial baseline. Panels show annual-mean differences relative to the preindustrial (Late Holocene) baseline (Osman et al., 2021). Note that plioDA sea ice is used for the Annan et al. (2024) reconstruction.

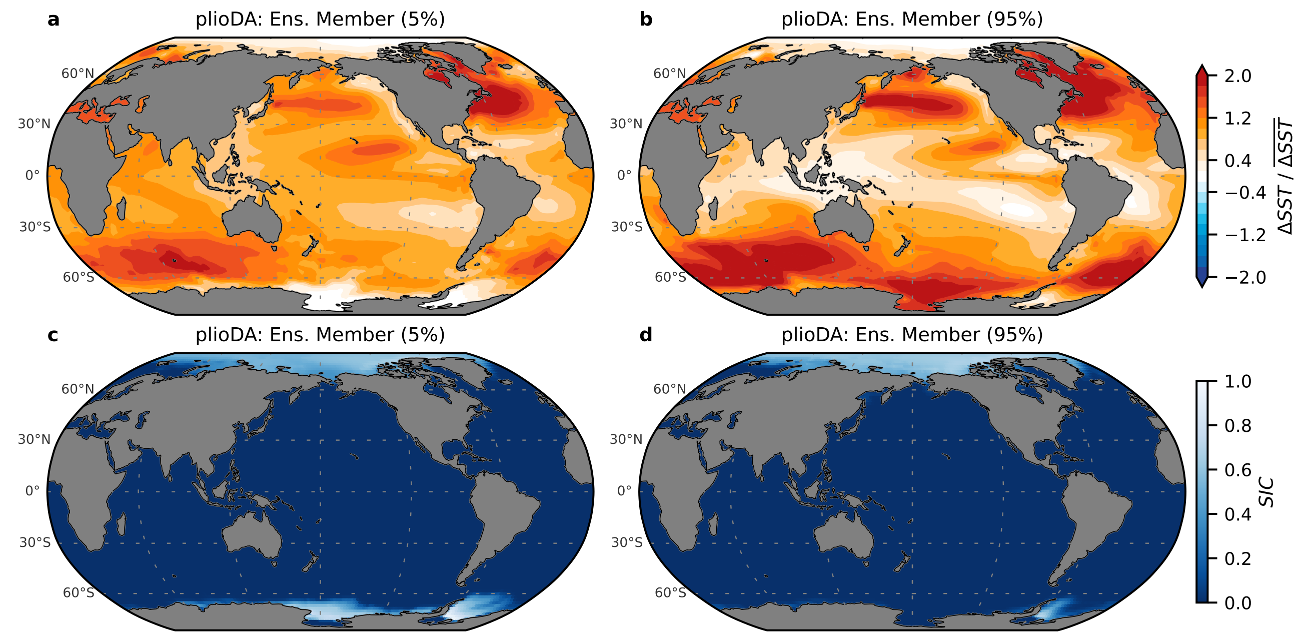

Figure S4. **5th and 95th percentile ensemble members from plioDA reconstruction** (Tierney et al., 2025). **(a–b)** Sea-surface temperature (SST) anomalies and **(c–d)** sea-ice concentration (SIC) for ensemble members with the 5^{th} percentile net feedback (more negative, stable climate) and 95^{th} percentile net feedback (more positive, less stable climate). Ensemble members are ranked using CAM4 Green's functions (Dong et al., 2019).

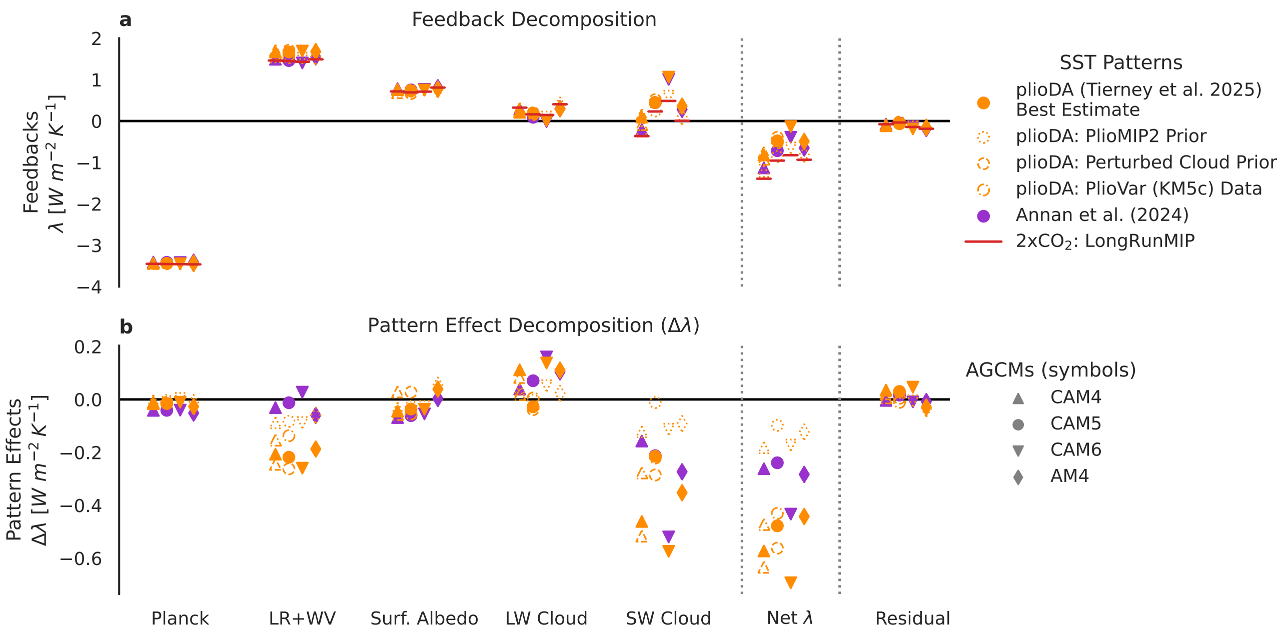

Figure S5. Kernel decomposition of radiative feedbacks (λ). Note that each legend applies to both panels: different sea-surface temperature and sea ice patterns are distinguished by colors/borders, while the different atmospheric general circulation models (AGCMs) are distinguished by symbol shapes. **(a)** Decomposition of feedbacks using radiative kernels (Soden et al., 2008) from CAM5 (Pendergrass et al., 2018). LR+WV represents the lapse rate and water vapor feedbacks. **(b)** Pattern effects ($\Delta\lambda = \lambda_{2\mathrm{xCO_2}} - \lambda_{\mathrm{Plio}}$) for each component feedback in panel **a**.

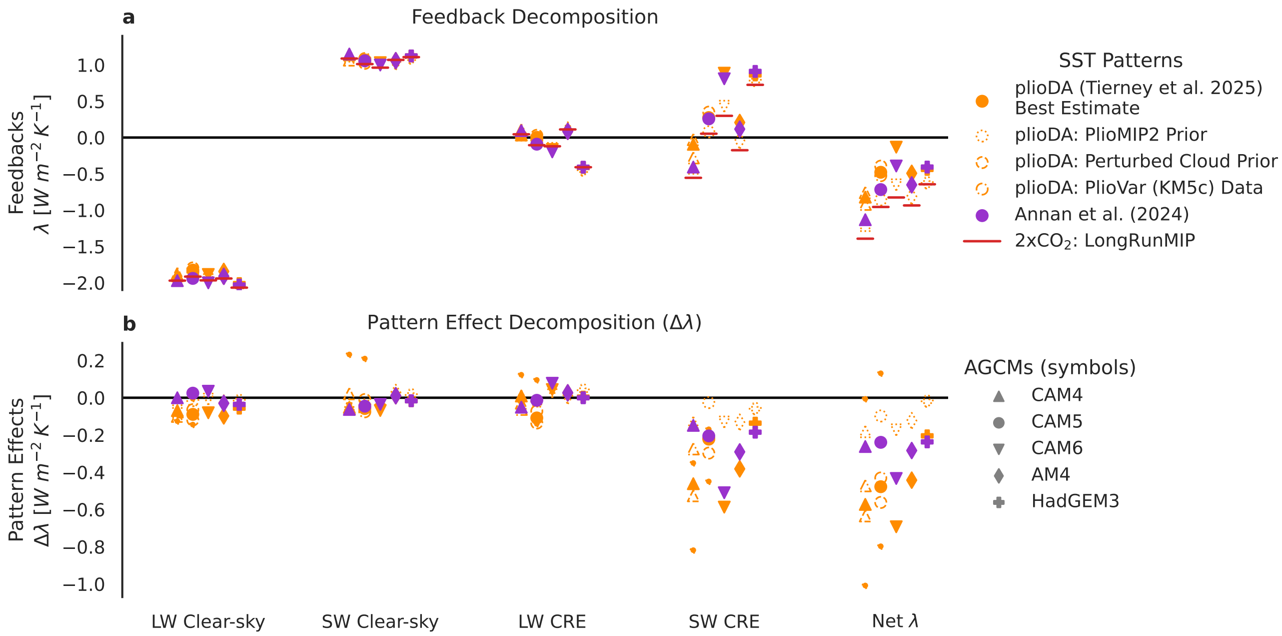

Figure S6. Decomposition of radiative feedbacks (λ) from direct model outputs for clear-sky radiation and cloud radiative effects (CRE). Results are separated into longwave (LW) and shortwave (SW) components. **(a)** Decomposition of feedbacks, and **(b)** decomposition of pattern effects ($\Delta\lambda = \lambda_{2xCO_2} - \lambda_{Plio}$).

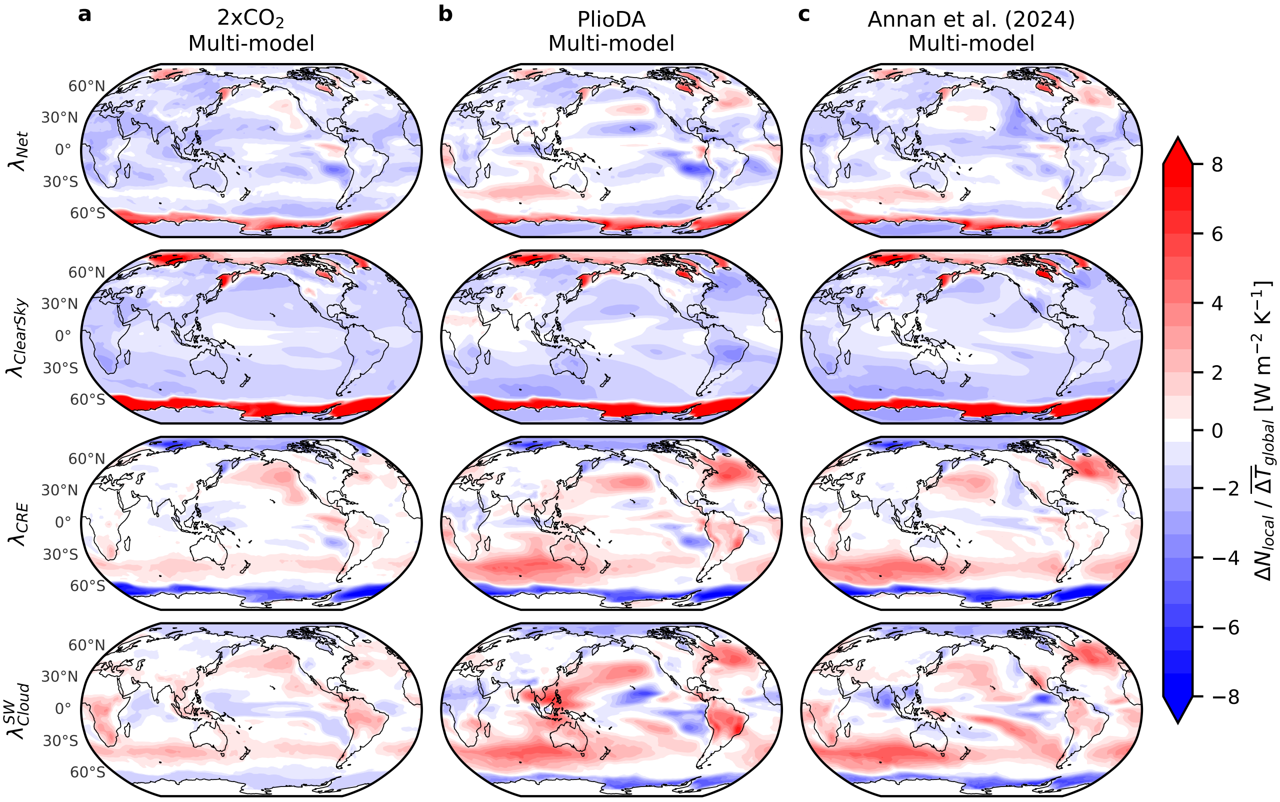

Figure S7. Spatial pattern of local radiative feedbacks (λ). Local feedbacks are calculated as $\Delta N/\overline{\Delta T}$, where ΔN is the local anomaly in top-of-atmosphere radiation, and $\overline{\Delta T}$ is the global-mean anomaly in near-surface air temperature. Multi-model mean, including CAM4, CAM5, CAM6, and GFDL-AM4 from **(a)** LongRunMIP $2xCO_2$ (Rugenstein et al., 2019), **(b)** plioDA (Tierney et al., 2025), and **(c)** Annan et al. (2024).

Figure S8–S9. Zonal mean of local radiative feedbacks (λ) and pattern effects, $\Delta\lambda = \lambda_{2xCO_2} - \lambda_{Plio}$, shown on the following pages. Local feedbacks are calculated as $\Delta N/\overline{\Delta T}$, where ΔN is the local anomaly in top-of-atmosphere radiation, and $\overline{\Delta T}$ is the global-mean anomaly in near-surface air temperature. **(a)** Feedbacks, λ, in CAM5 using various patterns of sea-surface temperature (SST) and sea ice, and **(b)** Pattern effects, $\Delta\lambda = \lambda_{2xCO_2} - \lambda_{Plio}$, in CAM5 corresponding to panel **a**. **(c–d)** Repeat of panels **a–b** with results from multiple models (CAM4, CAM5, CAM6, and GFDL-AM4) and a subset of SST and sea ice patterns.

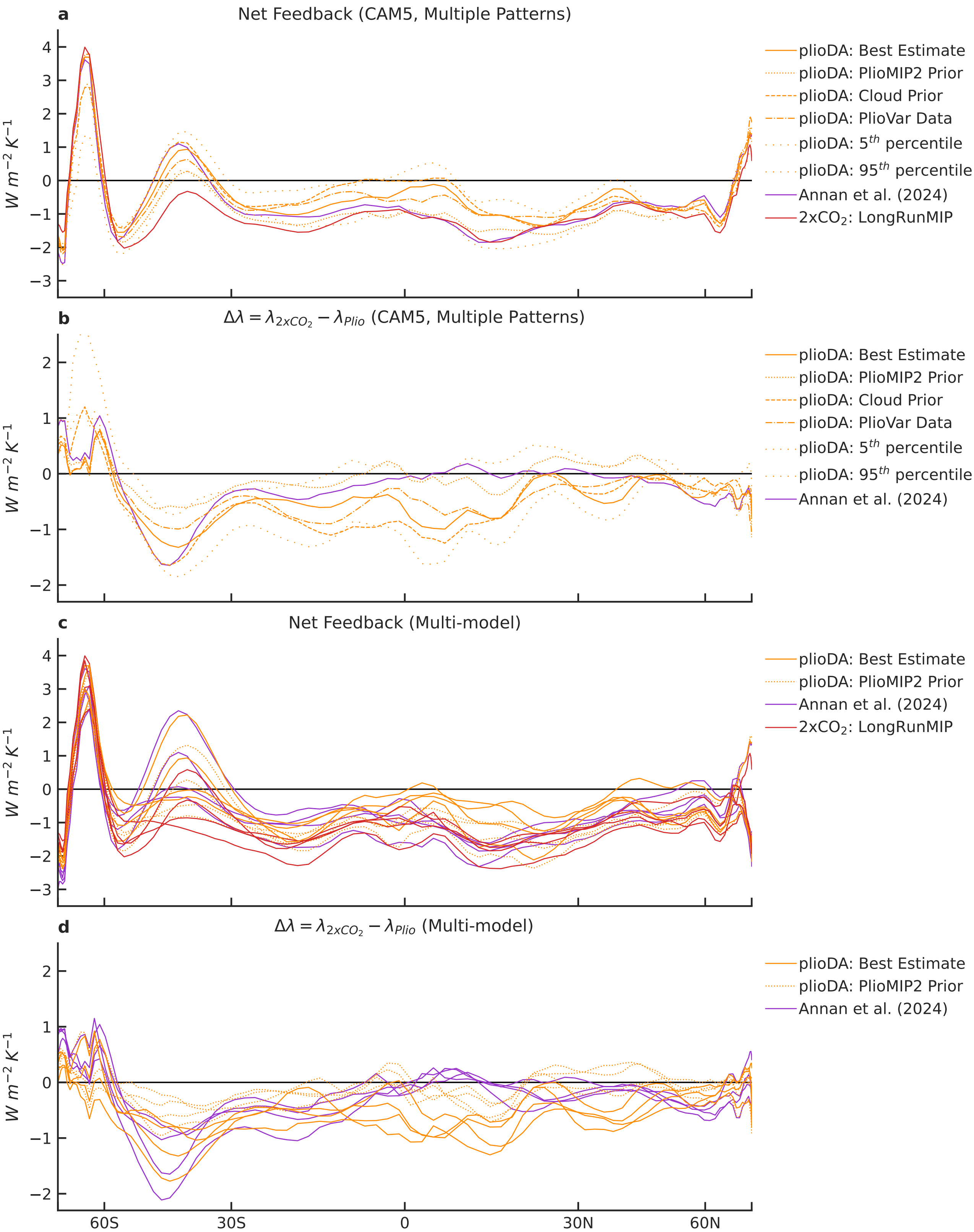

Figure S8. See caption on preceding page.

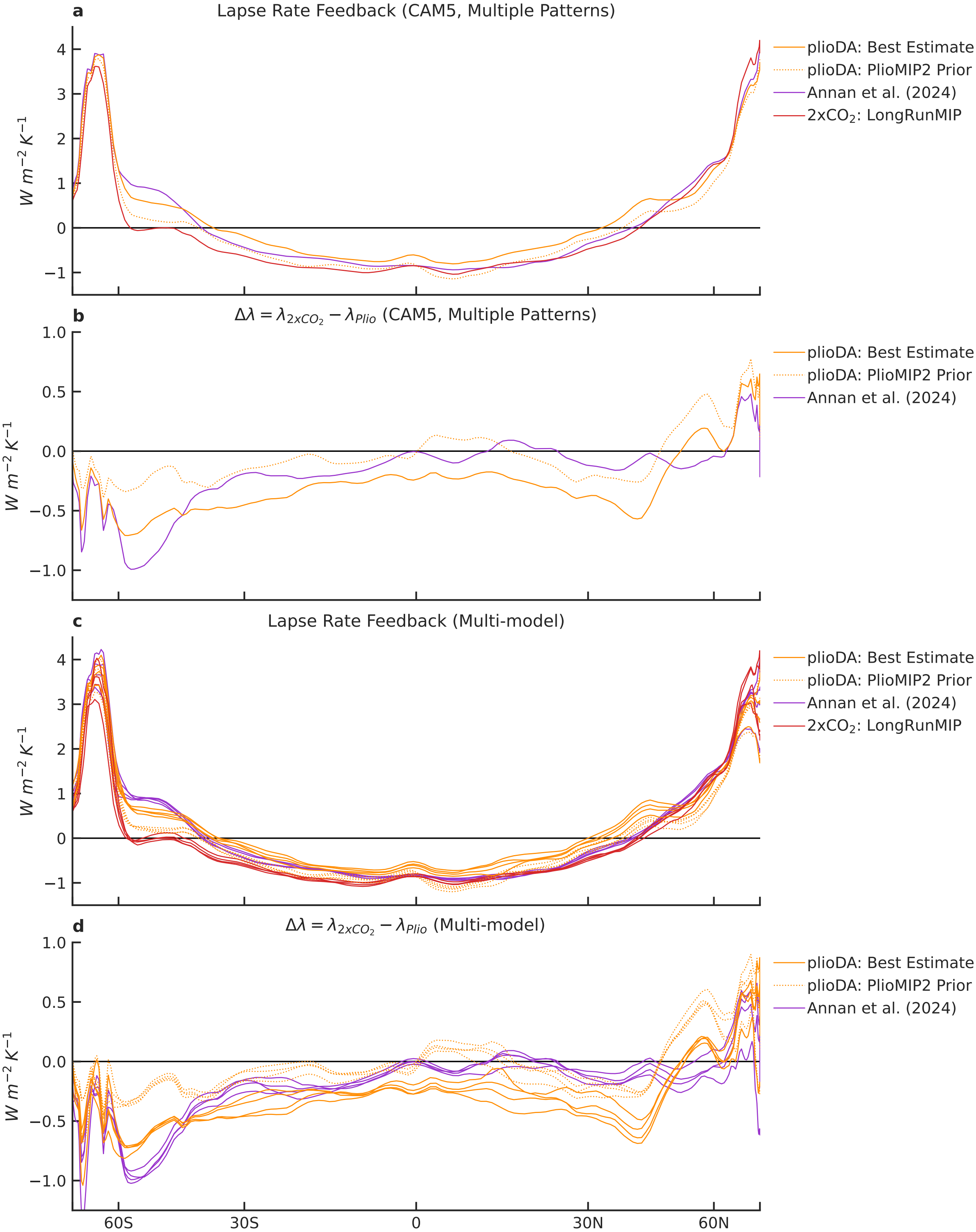

Figure S9. See caption that precedes Figure S8.

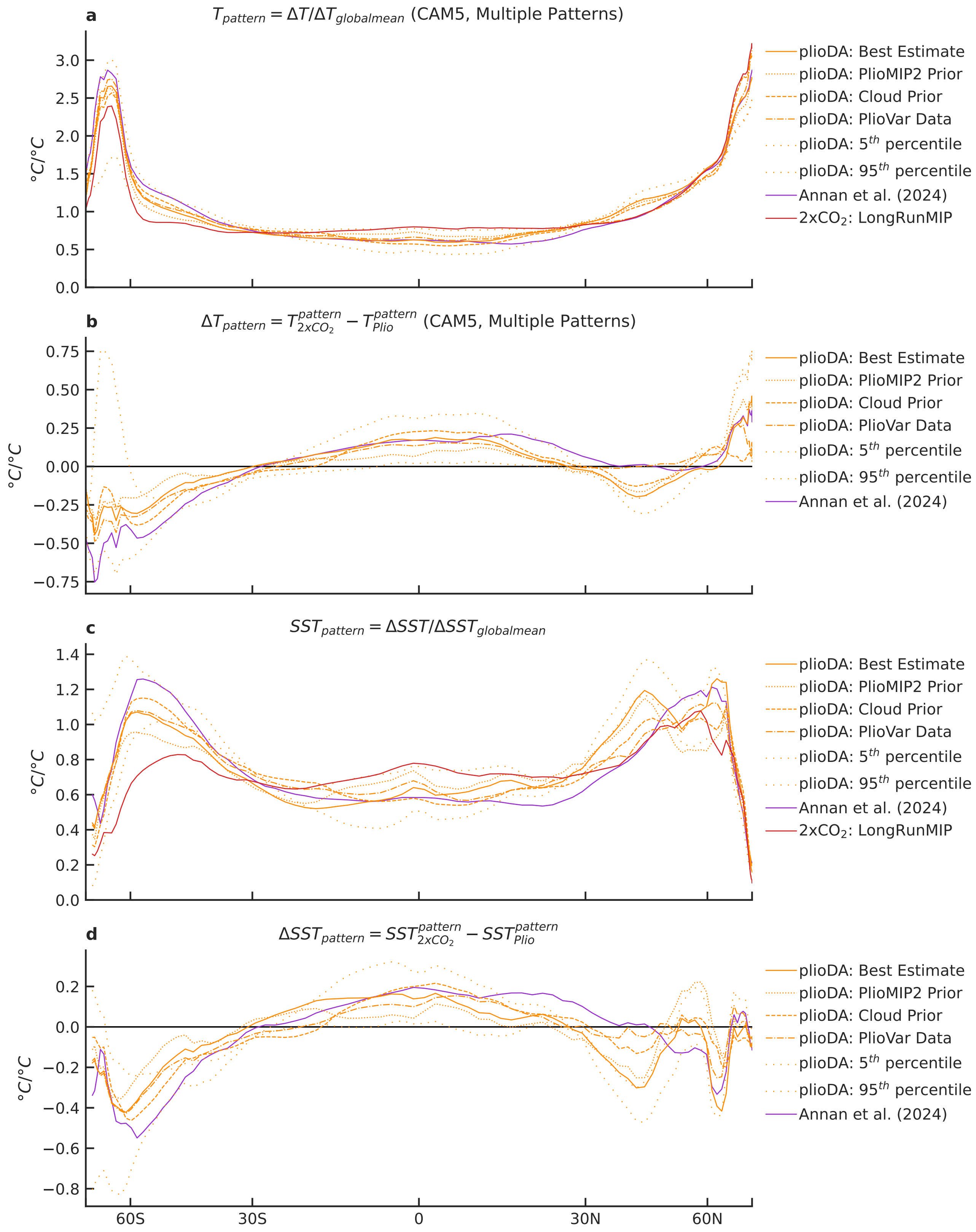

Figure S10. Zonal-mean patterns of temperature anomalies. **(A)** Normalized T from various patterns and **(b)** differences versus LongRunMIP 2xCO_2 pattern. **(c–d)** Repeats panels **a** and **b** for SST. Note that **a–b** show AGCM output from CAM5, whereas **c–d** show input boundary conditions for all AGCMs.

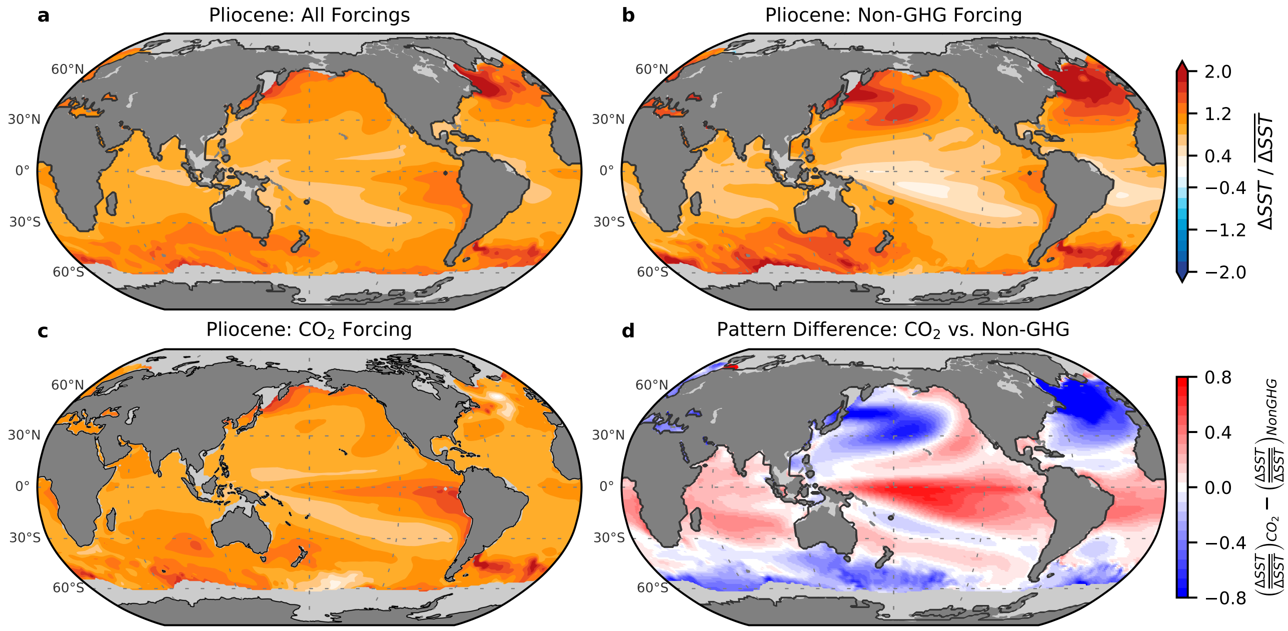

Figure S11. Sea-surface temperature (SST) response to Pliocene forcings in CESM2.1. Results shown are from (Dvorak et al., 2025). **(a–c)** Patterns of SST anomalies (normalized by global-mean anomalies) relative to preindustrial control from **(a)** all Pliocene forcings, **(b)** Non-GHG forcings including ice sheets, vegetation, topography, and bathymetry, and **(c)** CO_2 concentration of 400 ppm, which accounts for both CO_2 and methane forcing. **(d)** Difference between SST response to CO_2 versus non-GHG forcing, represented as panel **c** minus panel **b**; red regions indicate stronger relative amplification of warming from CO_2, while blue regions indicate stronger relative amplification from non-GHG forcings. In all panels, regions of preindustrial sea ice are masked in light gray. The CESM2 simulations follow the PlioMIP2 protocol (Haywood et al., 2020; Feng et al., 2022).

Table S1. All units are W m^{-2} K^{-1}. Pliocene pattern effects, $\Delta\lambda = \lambda_{2xCO_2} - \lambda_{Plio}$, from three patterns of reconstructed Pliocene SST and sea ice in various AGCMs (CAM4 coupled to CLM4.5, CAM5.3 coupled to CLM5.0, CAM6.0 coupled to CLM5.0, GFDL-AM4.0, and HadGEM3-GC3.1-LL). Alternate values for Pliocene pattern effects, $\Delta\lambda^{Alt}_{150yr} = \lambda^{CO_2}_{150yr} - \lambda_{Plio}$, are shown using 150-yr regression of abrupt-4xCO$_2$ simulations (abrupt2xCO$_2$ for CAM6.0) from coupled models corresponding to each AGCM (Andrews et al., 2022).

Model	Pattern	$\Delta\lambda$	λ_{Plio}	λ_{2xCO_2}	$\Delta\lambda^{Alt}_{150yr}$	$\lambda^{CO_2}_{150yr}$
CAM4	plioDA	-0.57	-0.82	-1.39	-0.41	-1.23
CAM4	plioDA: PlioMIP2 Prior	-0.18	-1.21	-1.39	-0.02	-1.23
CAM4	Annan24	-0.26	-1.13	-1.39	-0.10	-1.23
CAM5	plioDA	-0.48	-0.48	-0.96	-0.67	-1.15
CAM5	plioDA: PlioMIP2 Prior	-0.10	-0.86	-0.96	-0.29	-1.15
CAM5	Annan24	-0.24	-0.72	-0.96	-0.43	-1.15
CAM6	plioDA	-0.69	-0.13	-0.83	-1.08	-1.21
CAM6	plioDA: PlioMIP2 Prior	-0.17	-0.65	-0.83	-0.56	-1.21
CAM6	Annan24	-0.43	-0.39	-0.83	-0.82	-1.21
GFDL-AM4	plioDA	-0.44	-0.49	-0.93	-0.37	-0.86
GFDL-AM4	plioDA: PlioMIP2 Prior	-0.12	-0.81	-0.93	-0.05	-0.86
GFDL-AM4	Annan24	-0.28	-0.65	-0.93	-0.21	-0.86
HadGEM3	plioDA	-0.20	-0.44	-0.64	-0.19	-0.63
HadGEM3	plioDA: PlioMIP2 Prior	-0.02	-0.62	-0.64	-0.01	-0.63
HadGEM3	Annan24	-0.24	-0.41	-0.64	-0.22	-0.63
CAM4	mean	-0.34	-1.05	-1.39	-0.18	-1.23
CAM5	mean	-0.27	-0.68	-0.96	-0.47	-1.15
CAM6	mean	-0.43	-0.39	-0.83	-0.82	-1.21
GFDL-AM4	mean	-0.28	-0.65	-0.93	-0.21	-0.86
HadGEM3	mean	-0.15	-0.49	-0.64	-0.14	-0.63
mean	Annan24	-0.29	-0.66	-0.95	-0.36	-1.02
mean	plioDA	-0.48	-0.47	-0.95	-0.54	-1.02
mean	plioDA: PlioMIP2 Prior	-0.12	-0.83	-0.95	-0.18	-1.02
mean	**mean**	-0.30	-0.65	-0.95	-0.36	-1.02
1σ	1σ 0.19	0.29		0.31		

Table S2. Pliocene pattern effects, $\Delta\lambda = \lambda_{2xCO_2} - \lambda_{Plio}$, from various patterns of reconstructed Pliocene SST and sea ice in CAM4 and CAM5. Global-mean anomalies for SST, near-surface air temperature (T), and top-of-atmosphere radiative imbalance (N) are shown for reference. Alternate values for Pliocene pattern effects, $\Delta\lambda^{Alt}_{150yr} = \lambda^{CO_2}_{150yr} - \lambda_{Plio}$, are shown using 150-yr regression feedbacks (Table S1).

Units		$Wm^{-2}K^{-1}$	$Wm^{-2}K^{-1}$	K	K	Wm^{-2}	$Wm^{-2}K^{-1}$
Model	Pattern	$\Delta\lambda$	λ	ΔSST	ΔT	ΔN	$\Delta\lambda^{Alt}_{150yr}$
CAM4	plioDA	-0.57	-0.82	3.00	3.90	-3.20	-0.41
CAM4	plioDA: PlioVar Data	-0.47	-0.92	2.89	3.78	-3.48	-0.31
CAM4	plioDA: PlioMIP2 Prior	-0.18	-1.21	2.94	3.86	-4.67	-0.02
CAM4	plioDA: Cloud Prior	-0.63	-0.76	2.83	3.68	-2.79	-0.47
CAM4	plioDA: 5%	-0.01	-1.39	3.96	4.88	-6.77	0.16
CAM4	plioDA: 95%	-1.01	-0.38	3.29	4.02	-1.55	-0.85
CAM4	Annan24	-0.26	-1.13	2.82	3.72	-4.21	-0.10
CAM4	**mean**	-0.45	-0.94	3.10	3.98	-3.81	-0.29
CAM4	**1σ**	0.33	0.33	0.41	0.41	1.65	0.33
CAM4	*2xCO2: LongRunMIP*		-1.39	2.35	3.16	-4.40	

Model	Pattern	$\Delta\lambda$	λ	ΔSST	ΔT	ΔN	$\Delta\lambda^{Alt}_{150yr}$
CAM5	plioDA	-0.48	-0.48	3.00	3.98	-1.90	-0.67
CAM5	plioDA: PlioVar Data	-0.43	-0.53	2.89	3.85	-2.02	-0.62
CAM5	plioDA: PlioMIP2 Prior	-0.10	-0.86	2.94	3.96	-3.40	-0.29
CAM5	plioDA: Cloud Prior	-0.56	-0.39	2.83	3.75	-1.48	-0.76
CAM5	plioDA: 5%	0.13	-1.09	3.96	4.99	-5.42	-0.06
CAM5	plioDA: 95%	-0.80	-0.16	3.29	4.10	-0.65	-0.99
CAM5	Annan24	-0.24	-0.72	2.82	3.78	-2.71	-0.43
CAM5	**mean**	-0.35	-0.60	3.10	4.06	-2.51	-0.55
CAM5	**1σ**	0.31	0.31	0.41	0.43	1.55	0.31
CAM5	*2xCO2: LongRunMIP*		-0.96	2.35	3.21	-3.07	

Table S3. Posterior distributions of climate sensitivity (S). "Combined Evidence" assumes the Baseline Prior, $\lambda \sim \mathrm{Unif}(-10, 10)$ W m^{-2} K^{-1}, and includes Process Understanding, Historical Evidence, and Paleoclimate Evidence from the Last Glacial Maximum (LGM) and Pliocene. The Robust Range also combines lines of evidence but assumes a Uniform S Prior, $S \sim \mathrm{Unif}(0, 20)$ K (Sherwood et al., 2020). "Pliocene Only" considers only Pliocene evidence and assumes the Uniform S Prior. All uncertainties shown are 1σ values. Table structure is comparable to Table 10 of Sherwood et al. (2020).

Combined Evidence (Baseline Prior)	5th	17th	50th	83rd	95th	Mean	ΔT_{Plio}	ΔF^{Plio}_{NonGHG}	ΔT_{LGM}
SW20: Original	2.3	2.6	3.1	3.9	4.7	3.2	3.0 ± 1.0	f_{ESS}	-5 ± 1
+ Update ΔT_{LGM}	2.3	2.7	3.2	4.1	5.0	3.4	3.0 ± 1.0	f_{ESS}	-6 ± 1
+ Update ΔT_{Plio}	2.6	2.9	3.6	4.6	5.6	3.8	4.1 ± 0.6	f_{ESS}	-6 ± 1
+ Update ΔF^{Plio}_{NonGHG}	2.5	2.8	3.4	4.3	5.2	3.6	4.1 ± 0.6	1.7 ± 1.0	-6 ± 1
Include only LGM $\Delta\lambda$	2.3	2.6	3.0	3.7	4.4	3.2	4.1 ± 0.6	1.7 ± 1.0	-6 ± 1
Include only Pliocene $\Delta\lambda$	2.3	2.6	3.1	3.9	4.7	3.3	4.1 ± 0.6	1.7 ± 1.0	-6 ± 1
Full Update incl. Paleo $\Delta\lambda$	**2.1**	**2.4**	**2.8**	**3.4**	**4.0**	**2.9**	4.1 ± 0.6	1.7 ± 1.0	-6 ± 1
Alt. Update incl. Paleo $\Delta\lambda^{\mathrm{Alt}}_{\mathrm{150yr}}$	2.1	2.4	2.8	3.5	4.1	3.0	4.1 ± 0.6	1.7 ± 1.0	-6 ± 1

Combined, Robust Range (Unif. S Prior)	5th	17th	50th	83rd	95th	Mean	ΔT_{Plio}	ΔF^{Plio}_{NonGHG}	ΔT_{LGM}
SW20: Original Robust Range (Unif. S)	2.4	2.8	3.5	4.5	5.7	3.7	3.0 ± 1.0	f_{ESS}	-5 ± 1
+ Update ΔT, ΔF^{Plio}_{NonGHG} (Unif. S)	2.6	3.0	3.8	4.9	6.2	4.0	4.1 ± 0.6	1.7 ± 1.0	-6 ± 1
Full Update incl. Paleo $\Delta\lambda$ (Unif. S)	2.3	2.6	3.1	3.8	4.6	3.2	4.1 ± 0.6	1.7 ± 1.0	-6 ± 1
Alt. Update incl. Paleo $\Delta\lambda^{\mathrm{Alt}}_{\mathrm{150yr}}$ (Unif. S)	2.3	2.6	3.1	3.9	4.8	3.3	4.1 ± 0.6	1.7 ± 1.0	-6 ± 1

Pliocene Only (Unif. S Prior)	5th	17th	50th	83rd	95th	Mean	ΔT_{Plio}	ΔF^{Plio}_{NonGHG}
SW20: Original	1.6	2.4	4.0	6.8	10.1	4.7	3.0 ± 1.0	f_{ESS}
+ Update ΔT_{Plio}	2.9	3.8	5.6	8.6	12.3	6.3	3.0 ± 1.0	f_{ESS}
+ Update ΔF^{Plio}_{NonGHG}	2.5	3.2	4.7	7.4	11.2	5.4	4.1 ± 0.6	1.7 ± 1.0
Include Pliocene $\Delta\lambda$	1.9	2.4	3.8	7.2	12.9	5.0	4.1 ± 0.6	1.7 ± 1.0
Alt. Pliocene $\Delta\lambda^{\mathrm{Alt}}_{\mathrm{150yr}}$	1.8	2.4	3.8	8.3	14.8	5.3	4.1 ± 0.6	1.7 ± 1.0

Units in °C; ΔF units in W m^{-2}.

Table S4. Paired estimates of Pliocene and LGM pattern effects, which use similar methods for data assimilation and the same AGCMs. The pairs are used to estimate the Pearson correlation and covariance between estimates of Pliocene and LGM pattern effects (Cooper et al., 2024). For the standard $\Delta\lambda, r = 0.56$ and cov $= 0.0123$ [W m^{-2} K^{-1}]^2. For $\Delta\lambda^{\mathrm{Alt}}_{\mathrm{150yr}}$, $r = 0.87$ and cov $= 0.0562$ [W m^{-2} K^{-1}]^2. Table units are W m^{-2} K^{-1}. LGM results use updated CESM2.1 $\lambda^{\mathrm{Alt}}_{\mathrm{150yr}}$ in Table S1.

AGCM	Plio Pattern	LGM Pattern	$\Delta\lambda_{\mathrm{Plio}}$	$\Delta\lambda_{\mathrm{LGM}}$	$\Delta\lambda^{\mathrm{Alt150}}_{\mathrm{Plio}}$	$\Delta\lambda^{\mathrm{Alt150}}_{\mathrm{LGM}}$
CAM4	plioDA	LGMR	-0.57	-0.45	-0.41	-0.21
CAM5	plioDA	LGMR	-0.48	-0.31	-0.67	-0.41
CAM6	plioDA	LGMR	-0.69	-0.63	-1.08	-1.02
AM4	plioDA	LGMR	-0.44	-0.33	-0.37	-0.27
HadGEM3	plioDA	LGMR	-0.20	-0.27	-0.19	-0.29
CAM4	Annan	Annan	-0.57	-0.29	-0.10	-0.06
CAM5	Annan	Annan	-0.48	-0.09	-0.43	-0.18
CAM4	plioDA: Cloud Prior	LGMR	-0.63	-0.45	-0.47	-0.21
CAM5	plioDA: Cloud Prior	LGMR	-0.56	-0.31	-0.76	-0.41
CAM4	plioDA: Cloud Prior	lgmDA	-0.63	-0.69	-0.47	-0.45
CAM5	plioDA: Cloud Prior	lgmDA	-0.56	-0.51	-0.76	-0.61
CAM4	plioDA	lgmDA	-0.57	-0.69	-0.41	-0.45
CAM5	plioDA	lgmDA	-0.48	-0.51	-0.67	-0.61

References

Andrews, T., Bodas-Salcedo, A., Gregory, J. M., Dong, Y., Armour, K. C., Paynter, D., ... Liu, C. (2022, 9). On the Effect of Historical SST Patterns on Radiative Feedback. *Journal of Geophysical Research: Atmospheres*, *127*(18). Retrieved from https://onlinelibrary.wiley.com/doi/10.1029/2022JD036675 doi: 10.1029/2022JD036675

Annan, J. D., Hargreaves, J. C., Mauritsen, T., McClymont, E., & Ho, S. L. (2024, 9). Can we reliably reconstruct the mid-Pliocene Warm Period with sparse data and uncertain models? *Climate of the Past*, *20*(9), 1989–1999. Retrieved from https://cp.copernicus.org/articles/20/1989/2024/ doi: 10.5194/cp-20-1989-2024

Cooper, V. T., Armour, K. C., Hakim, G. J., Tierney, J. E., Osman, M. B., Proistosescu, C., ... Chmielowiec, P. (2024, 4). Last Glacial Maximum pattern effects reduce climate sensitivity estimates. *Science Advances*, *10*(16), 9461. Retrieved from https://www.science.org/doi/10.1126/sciadv.adk9461 doi: 10.1126/sciadv.adk9461

Dong, Y., Proistosescu, C., Armour, K. C., & Battisti, D. S. (2019, 9). Attributing Historical and Future Evolution of Radiative Feedbacks to Regional Warming Patterns using a Green's Function Approach: The Preeminence of the Western Pacific. *Journal of Climate*, *32*(17), 5471–5491. Retrieved from https://journals.ametsoc.org/view/journals/clim/32/17/jcli-d-18-0843.1.xml doi: 10.1175/JCLI-D-18-0843.1

Dvorak, M., Armour, K., Feng, R., Cooper, V., Zhu, J., Proistosescu, C., & Burls, N. (2025). Mid-Pliocene climate forcing, sea-surface temperature patterns, and implications for modern-day climate sensitivity. *Journal of Climate (in press).*. Retrieved from https://vtcooper.github.io/files/papers/Dvorak_Pliocene_JCli_accepted.pdf

Feng, R., Bhattacharya, T., Otto-Bliesner, B. L., Brady, E. C., Haywood, A. M., Tindall, J. C., ... Peltier, W. R. (2022, 3). Past terrestrial hydroclimate sensitivity controlled by Earth system feedbacks. *Nature Communications*, *13*(1), 1306. Retrieved from `https://www.nature.com/articles/s41467-022-28814-7` doi: 10.1038/s41467-022-28814-7

Haywood, A. M., Tindall, J. C., Dowsett, H. J., Dolan, A. M., Foley, K. M., Hunter, S. J., ... Lunt, D. J. (2020, 11). The Pliocene Model Intercomparison Project Phase 2: large-scale climate features and climate sensitivity. *Climate of the Past*, *16*(6), 2095–2123. Retrieved from `https://cp.copernicus.org/articles/16/2095/2020/` doi: 10.5194/cp-16-2095-2020

Osman, M. B., Tierney, J. E., Zhu, J., Tardif, R., Hakim, G. J., King, J., & Poulsen, C. J. (2021, 11). Globally resolved surface temperatures since the Last Glacial Maximum. *Nature*, *599*(7884), 239–244. Retrieved from `https://www.nature.com/articles/s41586-021-03984-4` doi: 10.1038/s41586-021-03984-4

Pendergrass, A. G., Conley, A., & Vitt, F. M. (2018). Surface and top-of-atmosphere radiative feedback kernels for CESM-CAM5. *Earth Syst. Sci. Data*, *10*, 317–324. Retrieved from `https://doi.org/10.5194/essd-10-317-2018` doi: 10.5194/essd-10-317-2018

Rugenstein, M., Bloch-Johnson, J., Abe-Ouchi, A., Andrews, T., Beyerle, U., Cao, L., ... Yang, S. (2019, 12). LongRunMIP: Motivation and Design for a Large Collection of Millennial-Length AOGCM Simulations. *Bulletin of the American Meteorological Society*, *100*(12), 2551–2570. Retrieved from `https://journals.ametsoc.org/view/journals/bams/100/12/bams-d-19-0068.1.xml` doi: 10.1175/BAMS-D-19-0068.1

Sherwood, S. C., Webb, M. J., Annan, J. D., Armour, K. C., Forster, P. M., Hargreaves, J. C.,

... Zelinka, M. D. (2020, 12). An Assessment of Earth's Climate Sensitivity Using Multiple Lines of Evidence. *Reviews of Geophysics*, *58*(4). Retrieved from https://onlinelibrary.wiley.com/doi/10.1029/2019RG000678 doi: 10.1029/2019RG000678

Soden, B. J., Held, I. M., Colman, R., Shell, K. M., Kiehl, J. T., & Shields, C. A. (2008, 7). Quantifying Climate Feedbacks Using Radiative Kernels. *Journal of Climate*, *21*(14), 3504–3520. Retrieved from http://journals.ametsoc.org/doi/10.1175/2007JCLI2110.1 doi: 10.1175/2007JCLI2110.1

Tierney, J. E., King, J., Osman, M. B., Abell, J. T., Burls, N. J., Erfani, E., ... Feng, R. (2025, 2). Pliocene Warmth and Patterns of Climate Change Inferred From Paleoclimate Data Assimilation. *AGU Advances*, *6*(1). Retrieved from https://agupubs.onlinelibrary.wiley.com/doi/10.1029/2024AV001356 doi: 10.1029/2024AV001356